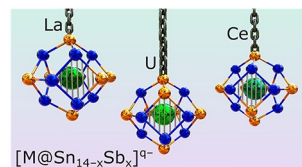


$[M@Sn_{14-x}Sb_x]^{q-}$ ($M = La, Ce, \text{ or } U; x = 6-8; q = 3, 4$): Interaction of 4f or 5f Metal Ions with 5p Metal Atoms in Intermetalloid Clusters

Katrin Beuthert, Bastian Weinert, Robert J. Wilson, Florian Weigend, and Stefanie Dehnen*

ABSTRACT: The impact of 4f metal ions Ln^{3+} ($Ln = La$ or Ce) versus 5f metal ions U^{n+} ($n = 3$ or 4) on the compositions and distribution of 5p metal atoms in the cluster shells of endohedral species $[M@Sn_{14-x}Sb_x]^{q-}$ ($M = La, Ce, \text{ or } U; x = 6-8; q = 3, 4$) was studied by means of combined experimental and quantum chemical investigations. While all known f-block metal ion-centered endohedral clusters possessed combinations of larger main group metal atoms so far (Sn/Bi or Pb/Bi), resulting in mixtures of 13- and 14-atom cages, the 14-atom cages reported herein comprise exclusively Sn and Sb atoms and therefore are challenged in accommodating the large 4f and 5f ions. We show that the clusters form in reactions of $(Sn_2Sb_2)^{2-}$ anions with $[Ln(C_5Me_4H)_3]$ or $[U(C_5Me_4H)_3Cl]$, and that salts of $[La@Sn_6Sb_8]^{3-}$, $[La@Sn_7Sb_7]^{4-}$, $[U@Sn_8Sb_6]^{4-}$, and $[U@Sn_7Sb_7]^{3-}$ can be isolated from them. The assignment of Sn versus Sb in the encapsulating cage follows a simple rule. Different central atoms cause only slight differences in this regard and with respect to distortions of the cluster shells. The reactions also yielded the salt of the new binary anion $(Sn_4Sb_4)^{2-}$ that was recently predicted by quantum chemical studies.



INTRODUCTION

The generation and in-depth investigation of binary and ternary intermetalloid clusters, in which a metal atom of the d-block or f-block is encapsulated by a cage of p-block metal atoms, have been two of the primary topics of metal cluster research for approximately two decades.¹⁻⁹ Ternary clusters in particular have been intensely studied by research groups worldwide because of the sheer endless variations of elemental combinations and structures, and the uncommon electronic properties resulting from their structural diversity.^{4,9-12} The comprehensive studies have revealed a large variety of bonding patterns,¹³ and clusters with combined d/p-block elemental combinations have meanwhile also been successfully used for catalytic reactions.¹⁴

However, most studies in this field have focused on clusters with d-block metal atoms in the interstitial position, while studies of the chemistry and physics of clusters with endohedral lanthanide or actinide atoms have remained scarce. The first intermetalloid cluster comprising an f-block metal ion within a cage of main group metal atoms was reported in 2011, $[Eu@Sn_6Bi_8]^{4-}$.¹⁵ The corresponding $[K(\text{crypt-222})]^+$ (crypt-222: 4,7,13,16,21,24-hexaoxa-1,10-diazabicyclo[8.8.8]-hexacosane) salt exhibited mainly ionic interactions between the inner Eu^{2+} ions and the binary cage. This was also proven by magnetic measurements indicating an unchanged $S = 7/2$ ground state of the Eu^{2+} ion.

Studies following this first report comprised comprehensive investigations of compounds with binary cluster shells of either Sn and Bi, Pb and Bi, Ga and Bi, or In and Bi atoms. The isolation of compounds with 13-atom shells, $[Sm@Ga_{3-x}H_{3-2x}Bi_{10+x}]^{3-}$ ($x = 0$ or 1),¹⁶ $[Ln@Pb_{13-x}Bi_x]^{q-}$ ($Ln = La, Ce, Nd, Gd, Sm, \text{ or } Tb; x/q = 9/4$ or $10/3$), $[Ln@$

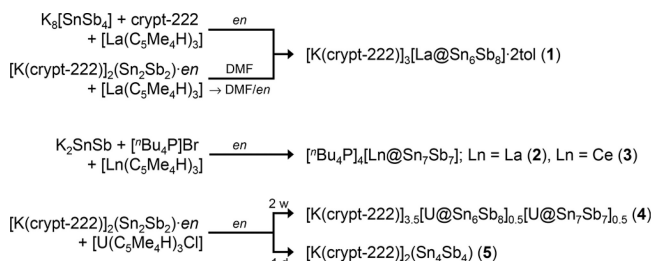
$Sn_4Bi_9]^{4-}$ ($Ln = La$ or Ce),^{17,18} $[U@Tl_2Bi_{11}]^{3-}$,¹⁹ and $[U@Pb_4Bi_9]^{3-}$,¹⁹ or 14-atom shells, $[Ln@Pb_{14-x}Bi_x]^{q-}$ ($Ln = La, Ce, Nd, Gd, Sm, \text{ or } Tb; x/q = 7/4$ or $8/3$), $[Ln@Sn_7Bi_7]^{4-}$ ($Ln = La$ or Ce),^{17,18} and $[U@Pb_7Bi_7]^{3-}$,¹⁹ or a doubly μ -Bi-bridged dimer of 13-atom cages, $\{[La@In_2Bi_{11}](\mu-Bi)_2[La@In_2Bi_{11}]\}^{6-}$,²⁰ indicated significantly lower yields for Sn/Bi and Ga/Bi elemental combinations. Larger cages in contrast, especially those comprising Pb and Bi atoms, are exceptionally well suited for accommodation of the large f-block metal ions. Quantum chemical studies were performed to further explore this observation, which confirmed that smaller cages can face steric problems.¹⁸

To date, the only f-block metal-centered clusters with a purely 5p-block metal environment have been $[Ln@Sb_{12}]^{3-}$ clusters ($Ln = La, Y, Ho, Er, \text{ or } Lu$),²¹ which are structurally related to their 5f/Bi analogues $[An@Bi_{12}]^{q-}$ ($An/q = Th/4$ or $U/3$).^{19,22} However, these clusters do not exhibit closed cluster shells but rather a doughnut-like 12-atom polycycle surrounding the inner ions. We were therefore interested in exploring the possibility of enclosing 4f and 5f metal ions within closed shells of smaller p-block metal atoms and for this chose the Sn/Sb combination for the first time.

Here, we report the success of this study for different synthetic approaches, namely, reactions of (a) K_8SnSb_4 and

crypt-222, (b) K_2SnSb and $[^{137}Bu_4P]Br$, or (c) $[K(crypt-222)]_2(Sn_2Sb_2) \cdot en$ with $[Ln(C_5Me_4H)_3]$ ($Ln = La$ or Ce) and $[U(C_5Me_4H)_3Cl]$ in ethane-1,2-diamine (*en*) or *N,N*-dimethylformamide (DMF). Upon layering with toluene, these reactions afforded single crystals of the new compounds $[K(crypt-222)]_3[La@Sn_6Sb_8] \cdot 2tol$ (1), $[^{137}Bu_4P]_4[M@Sn_7Sb_7]$ ($M = La$ for 2; $M = Ce$ for 3), $[K(crypt-222)]_{3.5}[U@Sn_6Sb_8]_{0.5}[U@Sn_7Sb_7]_{0.5}$ (4), and $[K(crypt-222)]_2(Sn_4Sb_4)$ (5) (see Scheme 1).

Scheme 1. Syntheses of 1–5 from Different Sn/Sb Sources and $[Ln(C_5Me_4H)_3]$ ($Ln = La$ or Ce) or $[U(C_5Me_4H)_3Cl]$ ^a



^aSingle crystals were obtained upon layering with toluene in all cases.

All compounds were received in single-crystal form with yields varying between 5% and 70%. Their structures were elucidated by means of single-crystal X-ray diffraction, and the elemental compositions, which for Sn and Sb cannot be determined from standard X-ray measurements, were determined by a combination of elemental analysis [micro-X-ray fluorescence spectroscopy (μ -XFS)] and quantum chemical studies employing density functional theory (DFT) methods.

EXPERIMENTAL SECTION

General. All syntheses were performed in the absence of air and moisture using standard Schlenk or glovebox techniques. Solvents and DMF were distilled from CaH_2 and stored over 3 Å molecular sieves. Toluene (tol, Acros Organics, 99%) was distilled from a sodium–potassium alloy and stored over 3 Å molecular sieves. Crypt-222 and $[^{137}Bu_4P]Br$ were dried in vacuum for at least 18 h. K_2SnSb was prepared by stoichiometric fusion of the elements at 950 °C for 48 h in a niobium tube, sealed within an evacuated silica ampule according to the literature.²³ $[K(crypt-222)]_2(Sn_2Sb_2) \cdot 2en$ was precipitated from a 2:1 *en* solution of crypt-222 and K_2SnSb upon addition of 5 equiv of toluene. K_8SnSb_4 was prepared according to the literature.²⁴ The complexes $[Ln(C_5Me_4H)_3]$ ($Ln = La$ or Ce) and $[U(C_5Me_4H)_3Cl]$ were synthesized as reported previously.^{17,19}

Preparation of $[K(crypt-222)]_3[La@Sn_6Sb_8] \cdot 2tol$ (1). $[K(crypt-222)]_2(Sn_2Sb_2) \cdot en$ (103 mg, 0.075 mmol) and $[La(C_5Me_4H)_3]$ (25 mg, 0.050 mmol) were combined in a Schlenk tube and dissolved in 2.5 mL of DMF. After the mixture had been stirred for 18 h at 60 °C, a dark brown powder precipitated from the dark red solution upon addition of 24 mL of toluene. The precipitate was washed three times with 5 mL of toluene. Then, it was redissolved in 2 mL of a 1:1 DMF/*en* mixture and filtered through a 0.45 μ m PTFE syringe filter. The black solution was layered with 6 mL of toluene and finally stored at 5 °C. After 2 months, small black, block-like crystals (yield of <5%) were present at the bottom of the Schlenk tube.

Another possibility is the reaction of K_8SnSb_4 (115 mg, 0.125 mmol), crypt-222 (380 mg, 1.00 mmol), and $[La(C_5Me_4H)_3]$ (82 mg, 0.163 mmol) in a mixture of 4 mL of *en* and 2 mL of toluene for 4.5 h at room temperature with stirring. The dark brown reaction mixture was filtered through a standard glass frit. The resulting reddish brown solution was layered with 4 mL of toluene. After 3 months, small black, block-like crystals (yield of <5%) were present in the wall of the Schlenk tube.

Preparation of $[^{137}Bu_4P]_4[La@Sn_7Sb_7]$ (2). K_2SnSb (51 mg, 0.16 mmol), $[^{137}Bu_4P]Br$ (109 mg, 0.35 mmol), and $[La(C_5Me_4H)_3]$ (27 mg, 0.054 mmol) were combined in a Schlenk tube and dissolved in 3 mL of *en*. After the mixture had been stirred for 10 min at room temperature, the dark red solution was sonicated for 1 h. Six milliliters of toluene was added, and the solution was stirred for 19 h. Then, it was filtered through a 0.45 μ m PTFE syringe filter. The black solution was stirred for an additional 3 h at 60 °C, filtered again through a 0.45 μ m PTFE syringe filter, layered with 8 mL of toluene, and finally stored at 5 °C. After 2 months, small black, block-like crystals (yield of <5%) were present at the bottom of the Schlenk tube.

Preparation of $[^{137}Bu_4P]_4[Ce@Sn_7Sb_7]$ (3). K_2SnSb (51 mg, 0.16 mmol), $[^{137}Bu_4P]Br$ (109 mg, 0.35 mmol), and $[Ce(C_5Me_4H)_3]$ (27 mg, 0.054 mmol) were combined in a Schlenk tube and dissolved in 4 mL of *en*. After the mixture had been stirred for 10 min at room temperature, the dark red solution was sonicated for 1 h. Six milliliters of toluene was added, and the solution was stirred for 20 h. Then, it was filtered through a 0.45 μ m PTFE syringe filter. The black solution was stirred for an additional 3 h at 60 °C, filtered again through a 0.45 μ m PTFE syringe filter, layered with 8 mL of toluene, and stored at 5 °C. After 3 months, large black, block-like crystals (yield of <5%) were present at the bottom of the Schlenk tube.

Preparation of $[K(crypt-222)]_{3.5}[U@Sn_{14-x}Sb_y]$ ($x = 7$ or 6 ; $y = 7$ or 8) (4) and $[K(crypt-222)]_2(Sn_4Sb_4)$ (5). $[K(crypt-222)]_2(Sn_2Sb_2) \cdot en$ (103 mg, 0.075 mmol) was dissolved in 3 mL of *en*, and the bright red solution was sonicated for 5 min. Then, a suspension of $[U(C_5Me_4H)_3Cl]$ (23 mg, 0.036 mmol) in 1 mL of *en* was added slowly. The dark red solution was stirred vigorously overnight at room temperature. The resulting dark brown solution was filtered through a 0.7 μ m PTFE syringe filter, carefully layered with 6 mL of toluene, and stored for crystallization at 5 °C. After 1 day, crystals of 5 (dark red blocks and orange sticks; yield of 75%) were visible in the Schlenk tube. After an additional 2 weeks, crystals of 4 (black blocks; yield of <5%) formed in the Schlenk tube.

Micro-X-ray Fluorescence Spectroscopy (μ -XFS). All μ -XFS measurements were performed on single-crystal samples with a Bruker M4 Tornado instrument, equipped with a Rh target X-ray tube, polycapillary optics, and a Si drift detector. The emitted fluorescence photons were detected with an acquisition time of 180 s. Quantification of the elements was achieved through deconvolution of the spectra. The results are summarized in Table S1. Figures S1–S5 present the spectra for 1–5, respectively. The results confirm the values observed by crystallography for 1–3 and 5. The results for 4 can be seen only as qualitative proof of the composition, because the signals of U-M overlay those of K, Sn, and Sb. Therefore, the deconvolution algorithm overinterprets the amount of U and underinterprets the amounts of the other elements.

Electrospray Ionization Mass Spectrometry (ESI-MS). ESI-MS in negative mode (ESI[−]) was carried out on a Thermo Fischer Scientific Finnigan LTQ-FT spectrometer in negative ion mode. The solutions were injected into the spectrometer with gastight 250 μ L Hamilton syringes by syringe pump infusion. All capillaries within the system were washed with a dry DMF mixture 2 h before, and at least 5 min between measurements was allowed to avoid decomposition reactions and consequent clogging. The following ESI parameters were used: spray voltage, 3.6 kV; capillary temperature, 290 °C; capillary voltage, −20 kV; tube lens voltage, −121.75 kV; sheath gas, 45; sweep gas, 0; auxiliary gas, 40. Assignable signals are summarized in Tables S2 and S3, and the ESI mass spectra are shown in Figures S6–S16.

Single-Crystal X-ray Diffraction. Crystals suitable for X-ray diffraction analyses were investigated with a Bruker D8 Quest diffractometer at 100 K using Mo $K\alpha$ radiation ($\lambda = 0.71073$ Å; 1–3) or with a STOE StadiVari diffractometer at 100 K using Cu $K\alpha$ radiation ($\lambda = 1.54186$ Å; 4 and 5). Upon multiscan absorption correction (APEX II for 1–3 and STOE LANA for 4 and 5), the structure solution was performed by dual-space methods, followed by full-matrix least-squares refinement against F^2 , using SHELXT15, SHELXT18/3, SHELXL15, SHELXL18/3, and OLEX2 software.^{25–27} Tables S4–S8 summarize the crystallographic data and

refinement results. Supplementary structural images are provided in Figures S17–S26.

Quantum Chemical Investigations. Density functional theory (DFT) calculations were performed with TURBOMOLE²⁸ using the TPSS functional²⁹ and employing def2-TZVP basis sets³⁰ for Sn, Sb, Pb, and Bi, together with Dirac–Fock effective core potentials.³¹ For La, Ce, and U, Wood–Boring type effective core potentials were used^{32–34} together with segmented contracted basis sets from the same references with slight modifications in the *g* function space, available as “def-TZVP” bases from ref 35. The conductor-like screening model³⁶ was used for charge compensation.

RESULTS AND DISCUSSION

Figure 1 shows the molecular structures of the cluster anions within compounds 1–4. Compound 1 crystallizes in

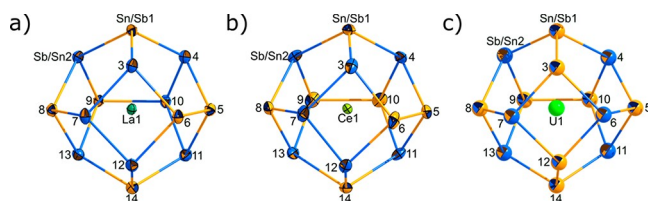


Figure 1. (a) Molecular structure of the $[\text{La}@\text{Sn}_6\text{Sb}_8]^{3-}$ anion in 1 (thermal ellipsoids at 50% probability), with selected interatomic distances: La–Sn/Sb, 3.3385(9)–3.4962(11) Å; Sn/Sb–Sn/Sb, 2.8544(8)–2.9280(10) Å. (b) Molecular structure of the $[\text{Ce}@\text{Sn}_7\text{Sb}_7]^{4-}$ anion in 3, as an example of the analogous anions in compounds 2 and 3 (thermal ellipsoids at 50% probability), with selected interatomic distances: Ce–Sn/Sb, 3.3152(5)–3.4745(6) Å; Sn/Sb–Sn/Sb, 2.8680(7)–2.9254(7) Å. (c) $[\text{U}@\text{Sn}_8\text{Sb}_6]^{3-}$ anion in 4 (spheres of arbitrary radii), with selected interatomic distances: U–Sn/Sb, 3.255(4)–3.472(4) Å; Sn/Sb–Sn/Sb, 2.817(6)–2.900(6) Å. As Sn and Sb atoms cannot be distinguished by means of common X-ray diffraction experiments, all atoms are shown as two-color octants, with the dominant (outer) color indicating the atom type that is more likely on the respective atomic position according to the DFT studies discussed below.

monoclinic space group $P2_1/n$ with four formula units in the unit cell. Compounds 2 and 3 crystallize in monoclinic space group $C2/c$ with one formula unit in the unit cell. Compound 4 crystallizes in tetragonal space group $P4_2bc$ with one formula unit in the unit cell (see Tables S4–S8 and Figures S17–S26).

As indicated in the Introduction, the observation of salts that comprise only one of the described cluster sizes, such as those observed in 1–4, is relatively rare and has so far been widely restricted to compounds with 13-atom cages, which comprised the smallest Ln^{3+} ions or group 13/15 shells.^{16,19,20} In contrast to the more common mixtures of 13- and 14-atom cages, which are observed for intermetallic clusters with Sn/Bi or Pb/Bi shells encapsulating endohedral lanthanide ions (see above),^{17,18} the clusters reported herein form exclusively 14-atom cages, which we ascribe to the smaller atomic radii of Sn and Sb. A similar steric reason caused the exclusive crystallization of the only other salt of an exclusive 14-atom cage anion with an elemental combination of $\text{Eu}^{2+}/\text{Sn}/\text{Bi}$, because of the larger ionic radius of the Eu^{2+} ion formed by *in situ* reduction,¹⁵ and the crystallization of two isostructural clusters with other elemental compositions comprising much smaller ions and atoms throughout, $[\text{M}@\text{Ge}_8\text{As}_6]^{3-}$ ($\text{M} = \text{Nb}$ or Ta).³⁷

The 14-atom cage that is observed in these clusters represents a nondeltahedral polyhedron with nine faces (six pentagonal ones and three square ones).^{38–41} It can be

constructed by cutting the three equatorial corners of a trigonal bipyramid, which indicates its high symmetry, as a rationale for its observation instead of a deltahedral 14-atom Frank–Kasper polyhedron, for instance. Due to its high, almost spherical symmetry (disregarding the occupation of the corners by different types of atoms), this topology apparently enjoys exceptional thermodynamic stability.

However, although they are isostructural and isoelectronic (with $70 = 5n$ valence electrons, where $n = 14$),^{13,42} the cluster shells of compounds 1–4 exhibit different ratios of the Sn and Sb atoms, which is required to adopt the overall charge of the cluster anion to the preferred amount of three $[\text{K}(\text{crypt-222})]^+$ counterions or four $[\text{K}(\text{crypt-222})]^+$ or $[\text{tBu}_4\text{P}]^+$ counterions, respectively, for crystallization. As the interstitial cations possess (formal) charges of 3+ (La or Ce) or 4+ (U), different amounts of formally Sn^- or Sb^0 (pseudo)group 15 atoms are thus required in the 14-atom shell to afford a total cluster charge (q) of 3– or 4–. For La^{3+} or Ce^{3+} , a Sn:Sb composition of 6:8 or 7:7 corresponds to the observed number of counterions in 1–3, as confirmed by μ -XFS measurements (Table S1 and Figures S1–S3). The uranium cluster in 4 exhibits a 1:1 mixture of cluster anions of both charges, and hence of clusters with a 7:7 and an 8:6 composition of Sn and Sb atoms, also in agreement with elemental analysis (Table S1 and Figure S4). Given these different compositions of the cluster shells, we were interested in seeing whether there are certain patterns in the distribution of the two types of 5p metal atoms at the 14 atomic positions.

The stability of this cluster architecture and the occupation of the corners with either Sn and Sb atoms when the interstitial ion is La^{3+} , Ce^{3+} , or U^{4+} were thus investigated by means of DFT (for computational details, see the Experimental Section). For a first impression of the potential energy surface, we calculated single-point energies for all distributions of Sn and Sb in $(\text{LaSn}_6\text{Sb}_8)^{3-}$ that are symmetry-distinct in a D_{3h} -symmetric topology of identical atoms. As listed in Table S10, the four most favorable isomers are found within an energy range of 10 kJ/mol, while the fifth is 17 kJ/mol above the most energetically favorable cluster. The energetically following 237 isomers are densely distributed between 28 and 162 kJ/mol, and the five most disfavored are between 168 and 185 kJ/mol. Common for the Sn/Sb distributions of the four energetically most favorable isomers is the occupation of the top and bottom positions (1 and 14, respectively, in Figure 1a) by Sn, and the occupation of at least two positions in each of the three equatorial rings by Sb, which leads to the maximum possible number of heteroatomic bonds, 16. Next, we treated the anions in 1–4 and, for comparison, also the corresponding clusters with a Pb/Bi shell (note that $[\text{La}@\text{Pb}_7\text{Bi}_7]^{4-}$ was computed earlier and served to predict the experimentally found species⁴³). All of them have 42 electrons in the valence p orbitals of the 14 shell atoms that form 21 two-electron, two-center bonds, which is evident from a Boys⁴⁴ localization procedure. For the targeted search of the best p element distributions, we applied a first-order perturbation theory in the nuclear charge^{43,45,46} to $[\text{M}@\text{Tt}_7\text{Pn}_7]^{q-}$ ($\text{Tt}/\text{Pn} = \text{Sn}/\text{Sb}$ or Pb/Bi ; $\text{M}/q = \text{La}/4$, $\text{Ce}/4$, or $\text{U}/3$), $[\text{M}@\text{Sn}_6\text{Sb}_8]^{3-}$ ($\text{M} = \text{La}$ or Ce), and $[\text{U}@\text{Sn}_8\text{Sb}_6]^{3-}$ (see Figure 2).

All obtained structures follow the distribution scheme formulated above. Furthermore, for the 7:7 composition, the most favorable distribution, $(7:7)^{\text{I}}$, is the same for $\text{M} = \text{La}$ and Ce and for $\text{Tt}/\text{Pn} = \text{Sn}/\text{Sb}$ and Pb/Bi ; the most favorable distribution for $[\text{U}@\text{Sn}_7\text{Sb}_7]^{3-}$, $(7:7)^{\text{II}}$, is very similar.

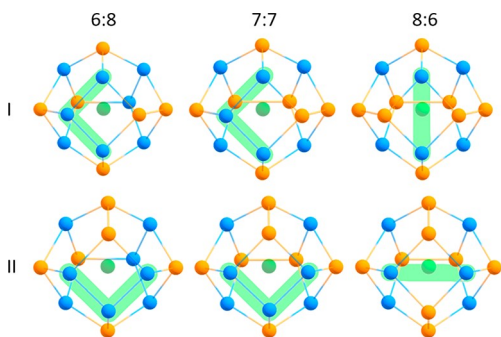


Figure 2. Energetically most favorable isomers found by perturbation theory in the nuclear charge. Arabic numerals indicate the Sn:Sb ratio (6:8, 7:7, or 8:6), and Roman numerals refer to the cluster type, I or II. Differences are colored green. For relative energies, see Table 1.

Consequently, the energy differences (for optimized structure parameters) between the two distributions are very small (see Table 1). For Ce and La, the most favorable isomers for a 6:8

Table 1. Relative Energies of the Energetically Most Favorable Isomers of $[M@Sn_{14-x}Sb_x]^{q-}$ [$M = La, Ce, \text{ or } U; x = 6-8$ (see Figure 2)] in Kilojoules per Mole

M	q	Sn/Sb		Pb/Bi	
		I	II	I	II
		7:7			
La	-4	0	0.1	0	1.6
Ce	-4	0	0.2	0	0.5
U	-3	1.8	0	2.4	0
		6:8			
La	-3	0	2.0	0	3.3
Ce	-3	0	2.1	0	2.4
		8:6			
U	-4	2.5	0	2.0	0

composition are achieved by replacing the Sn atom at position 10 (see Figure 1b) in (7:7)^I with Sb, and the most favorable distribution for $[U@Sn_8Sb_6]^{4-}$ is achieved by replacing the Sb atom at position 12 (see Figure 1b) in (7:7)^{II} with Sn. The same replacements for the almost isoenergetic isomers with higher energies with a 7:7 composition yield again almost isoenergetic isomers with compositions of 6:8 (La and Ce) and 8:6 (U). Thus, for 14-atom Tt/Pn cluster shells with 42 electrons in the valence p orbitals of the shell atoms, the distribution rule presented above, “Tt at top and bottom position, at least two Pn in each of the equatorial rings”, is robust, regardless of the elemental composition, regardless of whether the f occupation of the central ion is f⁰ (La), f¹ (Ce), or f² (U), and regardless of whether a lanthanide or an actinide resides in the center. As summarized in Table S11, the distances within the $\{Sn_{14-x}Sb_x\}$ cluster shells are subject to notable changes for different interstitial ions though, indicating the potential of these cages to “breathe” to a certain extent.

During the synthesis of compound 4, single crystals of compound 5 were isolated after shorter crystallization times (1 day instead of 2 weeks). It comprises binary $(Sn_4Sb_4)^{2-}$ anions (see Figure 3a,b), the architecture of which does not indicate a direct structural relationship with the cluster observed in 4. Hence, most likely, it is not an intermediate on the way toward the uranium-centered 14-atom cage in 4 but rather represents the product of a parallel pathway of cluster growth, which stops

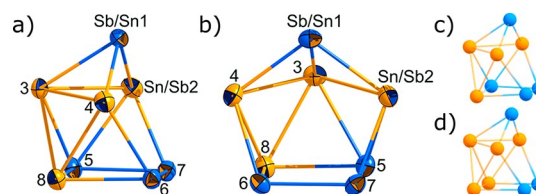


Figure 3. (a and b) Molecular structures of the $(Sn_4Sb_4)^{2-}$ anion in 5 in two views (thermal ellipsoids at 50% probability), with selected interatomic distances: Sb/Sn1–Sn/Sb2/3/4, 2.8294(5)–2.8569(5) Å; Sn/Sb2/3/4–Sn/Sb2/3/4, 3.2517(6)–3.32621(5) Å; Sn/Sb2/3/4–Sn/Sb5/6/7/8, 2.8322(4)–3.0548(4) Å; Sn/Sb5/6/7/8–Sn/Sb5/6/7/8, 2.7861(5)–2.8468(5) Å. As in Figure 1, all atoms are given as two-color octants, with the dominant color indicating the atom type that is more likely on the respective atomic position according to the DFT studies. The numbers refer to the respective atom labels and are also given in the color of the more probable atom at this position. (c) Calculated structures of the energetically most favorable isomer of the binary anion $(Sn_4Sb_4)^{2-}$. (d) Calculated structure of the energetically most favorable isomer of the binary anion $(Sn_5Sb_3)^{3-}$ for comparison.⁴⁷

at a convenient charge for crystallization with $[K(\text{crypt-222})]^+$ counterions (2– here). The composition of the anion, again not available through X-ray diffraction alone, was confirmed by μ -XFS measurements (Table S1 and Figure S5).

Notably, exactly this $(Sn_4Sb_4)^{2-}$ anion was recently predicted to exist by quantum chemical calculations in the context of another binary eight-atom anion comprising Sn and Sb atoms, $(Sn_5Sb_3)^{3-}$, which was obtained from K_2SnSb and $[^nBu_4P]Br$ in the absence of a Lewis-acidic f-block metal ion.⁴⁷ As observed for the f metal atom-centered clusters described above, the smaller $[^nBu_4P]^+$ cation tends to crystallize with similarly sized, more highly charged anions than do the larger $[K(\text{crypt-222})]^+$ cations (e.g., 4– in compound 2 vs in 3– in compound 1). Electrospray ionization mass spectrometry (ESI-MS) measurements of crystals of 5 (Figures S12–S16) indicate significant rearrangement processes in solution that also afford an anionic $\{Sn_5Sb_3\}$ fragment (detected as a monoanion, as usual), which obviously does not crystallize in the presence of $[K(\text{crypt-222})]^+$ cations though. Both binary anions are isoelectronic and possess the same topologies of a $2n + 6$ arachno type cage. The most energetically favorable isomers of both can be derived from a bicapped square antiprism, but the calculated structure with the lowest energy for $(Sn_4Sb_4)^{2-}$ is slightly distorted as compared to the more Sn-rich analogue, indicating the subtle differences between these two types of neighboring atoms and the limits of the pseudoelement concept at this point. The energetically most favorable isomers of the two anions as calculated with DFT methods are shown in panels c and d of Figure 3, respectively.

CONCLUSION

In summary, with this study, we improve our understanding of the family of intermetaloid clusters with 14-atom cages by presenting the first examples with purely 5p metal (Sn/Sb) cluster shells. As shown by quantum chemistry, interstitial Ln^{3+} or U^{4+} ions do not significantly affect the preferences of Sn and Sb atoms for occupying certain atomic positions in the cluster shell. Because of mainly ionic interactions, the relative stabilities of isomers with different Sn and Sb atom assignments are dominated by the stability of the respective main group cluster shells. However, small structural changes of the cluster shells are notable for the different interstitial

cations. The isolation of a second compound from the reaction with the uranium complex comprising a novel binary anion, $(\text{Sn}_4\text{Sb}_4)^{2-}$, provides important insight into the variance of the energy hypersurface in the reaction space of Sn/Sb-based Zintl anions and its diversity in the presence or absence of Lewis-acidic metal ions. At the same time, it confirmed a previously made theoretical prediction about the existence of this anion. Future studies will aim to use this new anion as a starting point for new ternary clusters.

AUTHOR INFORMATION

Corresponding Author

Stefanie Dehnen – *Fachbereich Chemie and Wissenschaftliches Zentrum für Materialwissenschaften (WZMW), Philipps-Universität Marburg, 35043 Marburg, Germany*; orcid.org/0000-0002-1325-9228;
Email: dehnen@chemie.uni-marburg.de

Authors

Katrin Beuthert – *Fachbereich Chemie and Wissenschaftliches Zentrum für Materialwissenschaften (WZMW), Philipps-Universität Marburg, 35043 Marburg, Germany*

Bastian Weinert – *Fachbereich Chemie and Wissenschaftliches Zentrum für Materialwissenschaften (WZMW), Philipps-Universität Marburg, 35043 Marburg, Germany*

Robert J. Wilson – *Fachbereich Chemie and Wissenschaftliches Zentrum für Materialwissenschaften (WZMW), Philipps-Universität Marburg, 35043 Marburg, Germany*

Florian Weigend – *Fachbereich Chemie and Wissenschaftliches Zentrum für Materialwissenschaften (WZMW), Philipps-Universität Marburg, 35043 Marburg, Germany*; orcid.org/0000-0001-5060-1689

Notes

The authors declare no competing financial interest.

ACKNOWLEDGMENTS

This work was supported by the Deutsche Forschungsgemeinschaft.

REFERENCES

(1) Fässler, T. F.; Hoffmann, S. D. Endohedral Zintl Ions: Intermetallic Clusters. *Angew. Chem., Int. Ed.* **2004**, *43*, 6242–6247.

(2) Fässler, T. F. Relationships Between Soluble Zintl Anions, Ligand-Stabilized Cage Compounds, and Intermetallic Clusters of Tetrel (Si–Pb) and Pentel (P–Bi) Elements. In *Zintl Ions: Principles and Recent Developments*; Fässler, T. F., Ed.; Springer: Berlin, 2011; pp 91–131.

(3) Scharfe, S.; Kraus, F.; Stegmaier, S.; Schier, A.; Fässler, T. F. Zintl Ions, Cage Compounds, and Intermetallic Clusters of Group 14 and Group 15 Elements. *Angew. Chem., Int. Ed.* **2011**, *50*, 3630–3670.

(4) Weinert, B.; Dehnen, S. Binary and Ternary Intermetallic Clusters. In *Clusters - Contemporary Insight in Structure and Bonding*; Dehnen, S., Ed.; Springer International Publishing: Cham, Switzerland, 2017; pp 99–134.

(5) Liu, C.; Popov, I. A.; Chen, Z.; Boldyrev, A. I.; Sun, Z.-M. Aromaticity and Antiaromaticity in Zintl Clusters. *Chem. - Eur. J.* **2018**, *24*, 14583–14597.

(6) Mayer, K.; Weßing, J.; Fässler, T. F.; Fischer, R. A. Intermetallic Clusters: Molecules and Solids in a Dialogue. *Angew. Chem., Int. Ed.* **2018**, *57*, 14372–14393.

(7) Weinert, B.; Mitzinger, S.; Dehnen, S. (Multi-)Metallic Cluster Growth. *Chem. - Eur. J.* **2018**, *24*, 8470–8490.

(8) Wilson, R. J.; Weinert, B.; Dehnen, S. Recent developments in Zintl cluster chemistry. *Dalton Trans.* **2018**, *47*, 14861–14869.

(9) Wilson, R. J.; Lichtenberger, N.; Weinert, B.; Dehnen, S. Intermetallic and Heterometallic Clusters Combining p-Block (Semi)Metals with d- or f-Block Metals. *Chem. Rev.* **2019**, *119*, 8506–8554.

(10) Perla, L. G.; Muñoz-Castro, A.; Sevov, S. C. Eclipsed- and Staggered- $[\text{Ge}_{18}\text{Pd}_3\{\text{E}^{\text{I}}\text{Pr}_3\}_6]^{2-}$ (E = Si, Sn): Positional Isomerism in Deltahedral Zintl Clusters. *J. Am. Chem. Soc.* **2017**, *139*, 15176–15181.

(11) Xu, Y.-H.; Tkachenko, N. V.; Popov, I. A.; Qiao, L.; Muñoz-Castro, A.; Boldyrev, A. I.; Sun, Z.-M. Ternary aromatic and antiaromatic clusters derived from the hypoh species $[\text{Sn}_2\text{Sb}_3]^{3-}$. *Nat. Commun.* **2021**, *12*, 4465.

(12) Pan, F.; Guggolz, L.; Weigend, F.; Dehnen, S. Atom Exchange Versus Reconstruction: $(\text{Ge}_x\text{As}_{4-x})^{x-}$ (x = 2, 3) as Building Blocks for the Supertetrahedral Zintl Cluster $[\text{Au}_6(\text{Ge}_3\text{As})(\text{Ge}_2\text{As}_2)_3]^{3-}$. *Angew. Chem., Int. Ed.* **2020**, *59*, 16638–16643.

(13) McGrady, J. E.; Weigend, F.; Dehnen, S. Electronic structure and bonding in endohedral Zintl clusters. *Chem. Soc. Rev.* **2022**, *51*, 628–649.

(14) Townrow, O. P. E.; Chung, C.; Macgregor, S. A.; Weller, A. S.; Goicoechea, J. M. A Neutral Heteroatomic Zintl Cluster for the Catalytic Hydrogenation of Cyclic Alkenes. *J. Am. Chem. Soc.* **2020**, *142*, 18330–18335.

(15) Lips, F.; Clérac, R.; Dehnen, S. $[\text{Eu}@\text{Sn}_6\text{Bi}_8]^{4-}$: A Mini-Fullerane-Type Zintl Anion Containing a Lanthanide Ion. *Angew. Chem., Int. Ed.* **2011**, *50*, 960–964.

(16) Weinert, B.; Müller, F.; Harms, K.; Clérac, R.; Dehnen, S. Origin and Location of Electrons and Protons during the Formation of Intermetallic Clusters $[\text{SmGa}_{3-x}\text{H}_{3-2x}\text{Bi}_{10+x}]^{3-}$ (x = 0, 1). *Angew. Chem., Int. Ed.* **2014**, *53*, 11979–11983.

(17) Lips, F.; Holyńska, M.; Clérac, R.; Linne, U.; Schellenberg, I.; Pöttgen, R.; Weigend, F.; Dehnen, S. Doped Semimetal Clusters: Ternary, Intermetallic Anions $[\text{LnSn}_7\text{Bi}_7]^{4-}$ and $[\text{LnSn}_4\text{Bi}_9]^{4-}$ (Ln = La, Ce) with Adjustable Magnetic Properties. *J. Am. Chem. Soc.* **2012**, *134*, 1181–1191.

(18) Ababei, R.; Massa, W.; Weinert, B.; Pollak, P.; Xie, X.; Clérac, R.; Weigend, F.; Dehnen, S. Ionic-Radius-Driven Selection of the Main-Group-Metal Cage for Intermetallic Clusters $[\text{LnPb}_x\text{Bi}_{14-x}]^{q-}$ and $[\text{LnPb}_y\text{Bi}_{13-y}]^{q-}$ (x/q = 7/4, 6/3; y/q = 4/4, 3/3). *Chem. - Eur. J.* **2015**, *21*, 386–394.

(19) Lichtenberger, N.; Wilson, R. J.; Eulenstein, A. R.; Massa, W.; Clérac, R.; Weigend, F.; Dehnen, S. Main Group Metal–Actinide Magnetic Coupling and Structural Response Upon U^{4+} Inclusion Into Bi, Tl/Bi, or Pb/Bi Cages. *J. Am. Chem. Soc.* **2016**, *138*, 9033–9036.

(20) Weinert, B.; Weigend, F.; Dehnen, S. Subtle Impact of Atomic Ratio, Charge and Lewis Basicity on Structure Selection and Stability:

- The Zintl Anion $[(\text{LaIn}_2\text{Bi}_{11})(\mu\text{-Bi})_2(\text{LaIn}_2\text{Bi}_{11})]^{6-}$. *Chem. - Eur. J.* **2012**, *18*, 13589–13595.
- (21) Min, X.; Popov, I. A.; Pan, F.-X.; Li, L.-J.; Matito, E.; Sun, Z.-M.; Wang, L.-S.; Boldyrev, A. I. All-Metal Antiaromaticity in Sb_4^- Type Lanthanocene Anions. *Angew. Chem., Int. Ed.* **2016**, *55*, 5531–5535.
- (22) Eulenstein, A. R.; Franzke, Y. J.; Lichtenberger, N.; Wilson, R. J.; Deubner, H. L.; Kraus, F.; Clérac, R.; Weigend, F.; Dehnen, S. Substantial π -aromaticity in the anionic heavy-metal cluster $[\text{ThBi}_{12}]^{4-}$. *Nat. Chem.* **2021**, *13*, 149–155.
- (23) Wilson, R. J.; Hastreiter, F.; Reiter, K.; Büschelberger, P.; Wolf, R.; Gschwind, R.; Weigend, F.; Dehnen, S. $[\text{Co}@\text{Sn}_6\text{Sb}_6]^{3-}$: An Off-Center Endohedral 12-Vertex Cluster. *Angew. Chem., Int. Ed.* **2018**, *57*, 15359–15363.
- (24) Eisenmann, B.; Klein, J. Na_5SnSb_3 und K_8SnSb_4 , Zwei neue Zintlphasen mit. *Z. Naturforsch. B* **1988**, *43*, 1156–1160.
- (25) Sheldrick, G. M. SHELXT – Integrated space-group and crystal-structure determination. *Acta Crystallogr., Sect. A* **2015**, *71*, 3.
- (26) Sheldrick, G. M. Crystal structure refinement with SHELXL. *Acta Crystallogr., Sect. C* **2015**, *71*, 3.
- (27) *Diamond - Crystal and Molecular Structure Visualization, Crystal Impact*; Dr. H. Putz & Dr. K. Brandenburg GbR, Bonn, Germany (<http://www.crystalimpact.com/diamond>).
- (28) TURBOMOLE, ver. 7.5 2020; a development of University of Karlsruhe and Forschungszentrum Karlsruhe GmbH, 1989–2007, TURBOMOLE GmbH, since 2007 (available from <http://www.turbomole.com>).
- (29) Tao, J.; Perdew, J. P.; Staroverov, V. N.; Scuseria, G. E. Climbing the Density Functional Ladder: Nonempirical Meta-Generalized Gradient Approximation Designed for Molecules and Solids. *Phys. Rev. Lett.* **2003**, *91*, 146401.
- (30) Weigend, F.; Ahlrichs, R. Balanced basis sets of split valence, triple zeta valence and quadruple zeta valence quality for H to Rn: Design and assessment of accuracy. *Phys. Chem. Chem. Phys.* **2005**, *7*, 3297–3305.
- (31) Metz, B.; Stoll, H.; Dolg, M. Small-core multiconfiguration-Dirac–Hartree–Fock-adjusted pseudopotentials for post-d main group elements: Application to PbH and PbO. *J. Chem. Phys.* **2000**, *113*, 2563.
- (32) Cao, X.; Dolg, M. Valence basis sets for relativistic energy-consistent small-core lanthanide pseudopotentials. *J. Chem. Phys.* **2001**, *115*, 7348.
- (33) Dolg, M.; Stoll, H.; Preuss, H. Energy-adjusted ab initio pseudopotentials for the rare earth elements. *J. Chem. Phys.* **1989**, *90*, 1730.
- (34) Cao, X.; Dolg, M.; Stoll, H. Valence basis sets for relativistic energy-consistent small-core actinide pseudopotentials. *J. Chem. Phys.* **2003**, *118*, 487–496.
- (35) <http://cosmologic-services.de/basis-sets/getbasis.ph>.
- (36) Schäfer, A.; Klamt, A.; Sattel, D.; Lohrenz, J. C. W.; Eckert, F. COSMO Implementation in TURBOMOLE: Extension of an efficient quantum chemical code towards liquid systems. *Phys. Chem. Chem. Phys.* **2000**, *2*, 2187–2193.
- (37) Mitzinger, S.; Broeckaert, L.; Massa, W.; Weigend, F.; Dehnen, S. Understanding of Multimetallic Cluster Growth. *Nat. Commun.* **2016**, *7*, 10480.
- (38) Grubisic, A.; Wang, H.; Ko, Y. J.; Bowen, K. H. Photoelectron spectroscopy of europium-silicon cluster anions, EuSi_n^- ($3 \leq n \leq 17$). *J. Chem. Phys.* **2008**, *129*, 054302.
- (39) Grubisic, A.; Ko, Y. J.; Wang, H.; Bowen, K. H. Photoelectron Spectroscopy of Lanthanide–Silicon Cluster Anions LnSi_n^- ($3 \leq n \leq 13$; Ln = Ho, Gd, Pr, Sm, Eu, Yb): Prospect for Magnetic Silicon-Based Clusters. *J. Am. Chem. Soc.* **2009**, *131*, 10783–10790.
- (40) Dognon, J.-P.; Clavaguéra, C.; Pyykkö, P. Towards a 32-Electron Principle: $\text{Pu}@\text{Pb}_{12}$ and Related Systems. *Angew. Chem., Int. Ed.* **2007**, *46*, 1427–1430.
- (41) Jin, X.; Arcisauskaite, V.; McGrady, J. E. The structural landscape in 14-vertex clusters of silicon, $\text{M}@\text{Si}_{14}$: when two bonding paradigms collide. *Dalton Trans.* **2017**, *46*, 11636–11644.
- (42) Mingos, D. M. P. Polyhedral skeletal electron pair approach. *Acc. Chem. Res.* **1984**, *17*, 311–319.
- (43) Weigend, F. Extending DFT-based genetic algorithms by atom-to-place re-assignment via perturbation theory: A systematic and unbiased approach to structures of mixed-metallic clusters. *J. Chem. Phys.* **2014**, *141*, 134103.
- (44) Boys, S. F. Construction of Some Molecular Orbitals to Be Approximately Invariant for Changes from One Molecule to Another. *Rev. Mod. Phys.* **1960**, *32*, 296–299.
- (45) Weigend, F.; Schrodt, C.; Ahlrichs, R. Atom distributions in binary atom clusters: A perturbational approach and its validation in a case study. *J. Chem. Phys.* **2004**, *121*, 10380–10384.
- (46) Weigend, F.; Schrodt, C. Atom-Type Assignment in Molecules and Clusters by Perturbation Theory-A Complement to X-ray Structure Analysis. *Chem. - Eur. J.* **2005**, *11*, 3559–3564.
- (47) Wilson, R. J.; Weigend, F.; Dehnen, S. The Arachno-Zintl Ion $(\text{Sn}_5\text{Sb}_3)^{3-}$ and the Effects of Element Composition on the Structures of Isoelectronic Clusters: Another Facet of the Pseudo-Element Concept. *Angew. Chem., Int. Ed.* **2020**, *59*, 14251–14255.